Long-range ordering effect in electrodeposition of zinc and zinc oxide

Tao Liu,[1] Sheng Wang,[1,*] Zi-liang Shi,[1] Guo-Bin Ma,[1] Mu Wang,[1,2,†] Ru-Wen Peng,[1] Xi-Ping Hao,[1] and Nai-ben Ming[1]

[1]*National Laboratory of Solid State Microstructures & Department of Physics, Nanjing University, Nanjing 210093, China*
[2]*International Center for Quantum Structures, Institute of Physics, Chinese Academy of Sciences, Beijing 100080, China*
(Received 16 November 2006; published 31 May 2007)

In this paper, we report the long-range ordering effect observed in the electro-crystallization of Zn and ZnO from an ultrathin aqueous electrolyte layer of $ZnSO_4$. The deposition branches are regularly angled, covered with random-looking, scalelike crystalline platelets of ZnO. Although the orientation of each crystalline platelet of ZnO appears random, transmission electron microscopy shows that they essentially possess the same crystallographic orientation as the single-crystalline zinc electrodeposit underneath. Based on the experimental observations, we suggest that this unique long-range ordering effect results from an epitaxial nucleation effect in electrocrystallization.

PACS number(s): 81.10.Aj, 81.15.Pq, 82.60.Nh, 82.45.Qr

I. INTRODUCTION

Pattern formation in electrochemical deposition has been studied for decades [1–17]. Among many areas of research, spatiotemporal oscillation in electrodeposition is of particular interest [18–28]. During electrodeposition of zinc, it has been observed that the electric current and voltage may spontaneously oscillate. The dynamic behavior of the electric current and voltage has been extensively investigated [19,23,28], and relations of the oscillating electric current and the periodic change of concentration field in front of growing zinc electrodeposits have been reported [28]. Recently, it has been observed in electrodeposition of copper that spontaneous, periodic oscillation of the electric signal is associated with the formation of periodic nanonodules on the deposit filaments [25,26]. In many cases the electrodeposits were polycrystalline, and there was no strong correlation among the crystallites in the branches. For this reason, in many previous studies, electrodeposition was regarded as a polycrystalline aggregation process, where deposit morphology was controlled by the macroscopic Laplacian fields, such as the electric and concentration fields. However, in previous studies people did find a few systems in which the electrodeposits tended to be single crystalline [28–30]. This is an important feature that may lead to a long-range ordering effect in electrodeposition.

On the other hand, in electrodeposition of metal from aqueous electrolytes, very often the metal oxides are codeposited when the *p*H of the solution is not sufficiently low, or the oxygen dissolved in the electrolyte remains in a high concentration [21,25,26]. People may intentionally change the electrode potential periodically to generate nanostructures of the metal and metal oxide [21]. Since the metal oxide and metal have different structural parameters and electric properties, it is interesting to find out how the crystallites of metal and metal oxide nucleate in electrodeposition, and what the relation of the crystallographic orientation of these crystallites is.

In this paper, we report a unique long-range ordering effect observed in the electrocrystallization of zinc from an ultrathin aqueous electrolyte layer of $ZnSO_4$, which has not been reported before to the best of our knowledge. The deposit branches are regularly angled, covered with scalelike crystalline platelets of ZnO. Transmission electron microscopy (TEM) shows that, although orientation of each platelet of ZnO appears random, the platelets possess the same crystallographic orientation, and cluster along a branch of the electrodeposit. TEM studies indicate that the crystallographic orientations of the zinc trunk and the ZnO platelets are strongly correlated. Based on the experimental observations, we suggest that this unique self-organized long-range ordering effect in electrocrystallization could be explained by epitaxial nucleation [31,32] on specific facets of the crystallite.

II. EXPERIMENT

The electrodeposition was carried out in a cell made of two cleaned glass plates. The electrodes were two parallel, straight bars 8.0 mm apart and fixed on the bottom glass plate. The anode was made of a pure zinc wire (99.9%, ⊘0.5 mm) and the cathode was a graphite rod (⊘0.5 mm). The electrolyte of $ZnSO_4$ (0.05*M*, *p*H=4.5) was confined in the space between the upper and lower glass plates and the electrodes. The separation between the upper and the bottom glass plates was 70 μm, achieved by using spacers. The detail structure of the experimental setup was similar to that reported before [25,26]. The electrolyte solution was prepared by dissolving analytical reagent $ZnSO_4$ in deionized ultrapure water (Milli-Q Acdemic A10, electric resistivity 17.8 MΩ cm). No special treatments were applied to the glass plate surface except for conventional cleaning. A Peltier element was placed beneath the electrodeposition cell to control the temperature. Both the deposition cell and the Peltier element were sealed in a thermostat chamber. The electrolyte solution was solidified by cooling the deposition cell from the bottom. Nucleation of the ice of $ZnSO_4$ electrolyte initiated from the bottom glass plate. During the so-

---

*Present address: NSF Nano-scale Science and Engineering Center, 5130 Etcheverry Hall, University of California, Berkeley, CA 94720, USA.

†Author to whom correspondence should be addressed. Email address: muwang@nju.edu.cn

lidification process, $ZnSO_4$ was partially expelled from the solid (known as the segregation effect in crystallization [31,33]). Hence, the concentration of $ZnSO_4$ increased in front of the ice-electrolyte interface. It is known that the temperature at which an electrolyte solidifies (melting or solidification point) depends on the electrolyte concentration. For an electrolyte of $ZnSO_4$, the solidification temperature decreases when this concentration is increased. When thermodynamic equilibrium was eventually reached at the setting temperature ($-4\ °C$, for example), an ultrathin electrolyte layer with concentrated $ZnSO_4$ was trapped between the ice of electrolyte and the glass substrate. The thickness of this trapped layer depended on temperature and initial concentration of the electrolyte. Electrodeposition was carried out in this ultrathin, highly concentrated electrolyte layer of $ZnSO_4$. The concentration in this layer should not exceed the saturated concentration at $-4\ °C$, otherwise crystallites of $ZnSO_4$ will be generated due to supersaturation.

In order to achieve a flat, uniform ice-electrolyte interface, several melting-solidification cycles were repeated, so eventually only one or just a few ice nuclei survived in the system. Great care was taken in solidification to avoid the formation of cellular and dendritic ice-electrolyte interfaces. Usually, a very low solidification rate is applied. The solidification process was monitored with a research optical microscope (Orthoplan-pol, Leitz). The morphology of the electrodeposits was further observed and analyzed with a field-emission scanning electron microscope (FESEM) (LEO 1530VP) and a high-resolution transmission electron microscope (JOEL 2000).

When solidification of electrolyte has completed and an ultrathin film has been formed, a constant voltage (or current) is applied across the electrodes. Electrodeposits initiate from the cathode and develop on the glass plate. Figure 1(a) shows the scanning electron micrograph of the electrodeposits. One may see that all the sidebranches of the deposit possess nearly the same angle with respect to the main trunk. The inset in Fig. 1(a) demonstrates the statistics of the angle of the sidebranches and the main trunk. A distinct peak appears at 60°. Further observation indicates that the deposit branches are covered with randomly oriented crystalline platelets. Very often the platelets are clustered, periodically distributed on the electrodeposit branch, as shown in Fig. 1(b).

For electrodeposition with a galvanostatic mode, we find that the voltage across the electrodes oscillates spontaneously. The alternating voltage is shown in Fig. 2(a), and the Fourier transform of the voltage signal is illustrated in Fig. 2(b). The oscillation frequency depends on the electric current and the pH of the electrolyte. We observed that the oscillation frequency increases when the electric current becomes higher. The same tendency appears on increasing the pH of the electrolyte: the oscillation speeds up at higher pH values [34]. Indeed, the spontaneous oscillation of the current-voltage signal in zinc electrodeposition has been reported before by several groups [19,24]. The difference of our current results and previous ones is that in this report the thickness of the electrolyte layer has been restricted to a few hundreds of nanometers, which is much thinner than in previous systems. It is therefore unlikely that convection (in-
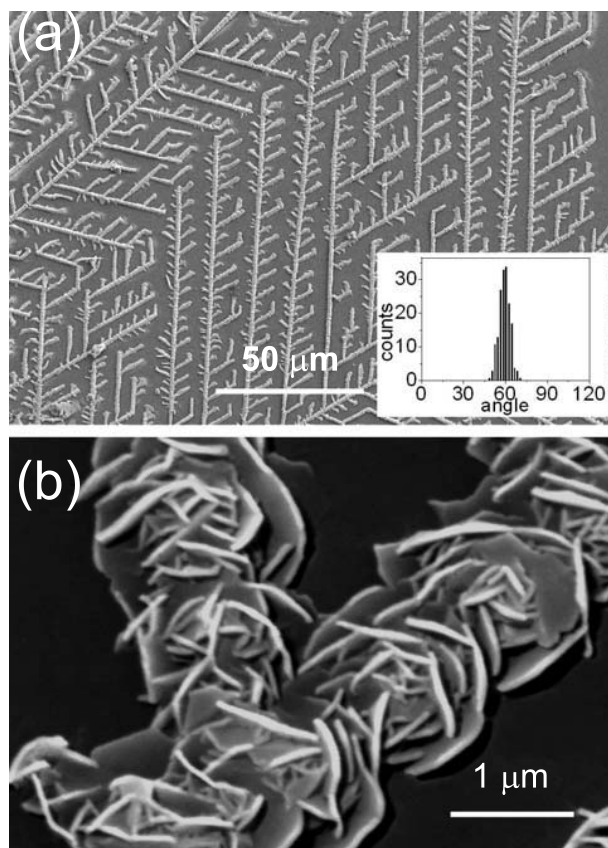
FIG. 1. (a) Scanning electron micrograph of the electrodeposit branches. The angle between the sidebranch and the main trunk is almost identical. The inset shows the statistics of the angle. A distinct peak appears at 60°. (b) The electrodeposit branch observed with higher magnification. The deposit branches are covered with random-looking crystalline platelets. Very often the platelets are clustered, forming a periodic structure along the electrodeposit branch.

cluding electroconvection) may play any role in initiating the spatiotemporal oscillation.

To find out the microstructure and hence possible formation mechanism of the peculiar electrodeposits shown in Fig. 1, transmission electron microscopy is used to identify the structure of the deposits. Figure 3(a) illustrates the diffraction contrast micrograph of the electrodeposits and Fig. 3(b) illustrates the electron diffraction pattern. Our analysis shows that two sets of diffraction spots can be identified. The diffraction spots marked by g_1 correspond to zinc, whereas the spots indicated by g_2 correspond to zinc oxide. The zone axes of these two sets of diffraction spots are both $[\bar{2}113]$, suggesting that zinc and zinc oxide take the same crystallographic orientation. Considering the fact that the size of the field diaphragm in electron microscopy is quite large, so a lot of crystallites are involved in the electron diffraction. Therefore, it is unexpected that the random-looking aggregates have such a well-defined single-crystal-like diffraction pattern. By very careful inspection of Fig. 3(b) one may also find that in addition to the two sets of distinct diffraction spots, there exists a very faint, diffused ring in between g_1 and g_2. Together with SEM micrographs and the diffraction
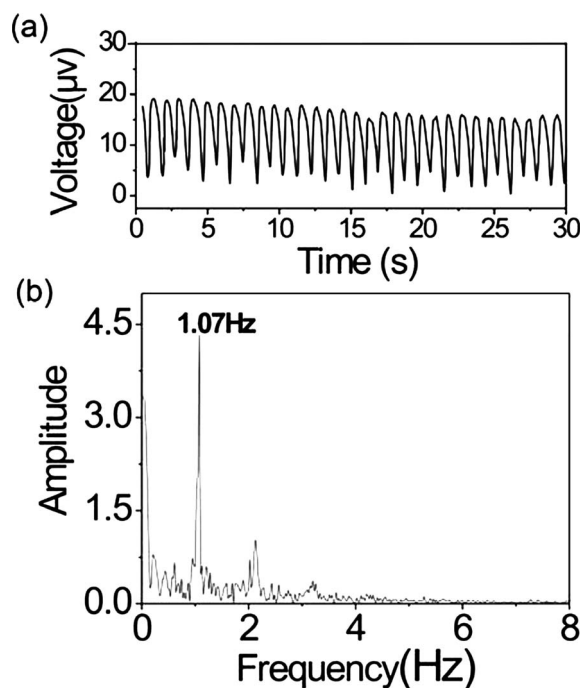
FIG. 2. (a) Alternating electric voltage recorded during the electrodeposition when a constant current is applied across the electrodes. Spontaneous, regular oscillation has been observed. The stable component in the voltage signal has been filtered in the measurement since we are more interested in the alternating component. (b) The Fourier transform of the alternating electric voltage signal, where distinct peaks can be identified.

contrast micrographs of the deposit, we expect that this faint ring may be contributed by some misoriented platelets of ZnO.

We need to point out that the amplitude of voltage oscillation shown in Fig. 2(a) is not large, yet the periodic structures on the deposit branches can be easily identified. A possible explanation is that the measured signal is contributed by all the deposit branches in the deposition cell. Once the separation of two growing tips is much larger than the thickness of the concentration boundary layer, then the local oscillation contributed by each deposit tip may not be exactly coherent. This may lead to the smaller oscillating amplitude in Fig. 2(a), despite the fact that the spatial periodicity on each electrodeposit branch is evident.

To identify the distribution of crystallites of zinc and zinc oxide in electrodeposits, we carry out energy-dispersive spectroscopy (EDS) experiment. In order to avoid the disturbance of chemical components in the glass substrate in EDS analysis, a freshly cleaned silicon wafer is used to replace the previous lower glass plate in the electrodeposition cell as the substrate (the transparent top glass plate is kept in order to monitor the nucleation process of ice). The silicon wafer with zinc electrodeposits was carefully washed with deioned water, dried in a nitrogen environment, and then mounted on a tiltable sample stage of the FESEM for measurements. Figure 4(a) shows the FESEM micrograph of the cross section of a deposit filament. It is clear that the filament consists of a compact kernel bounded with random-looking platelets. EDS analysis is carried out at sites *a*, *b*, and *c* in Fig. 4(a), respec-
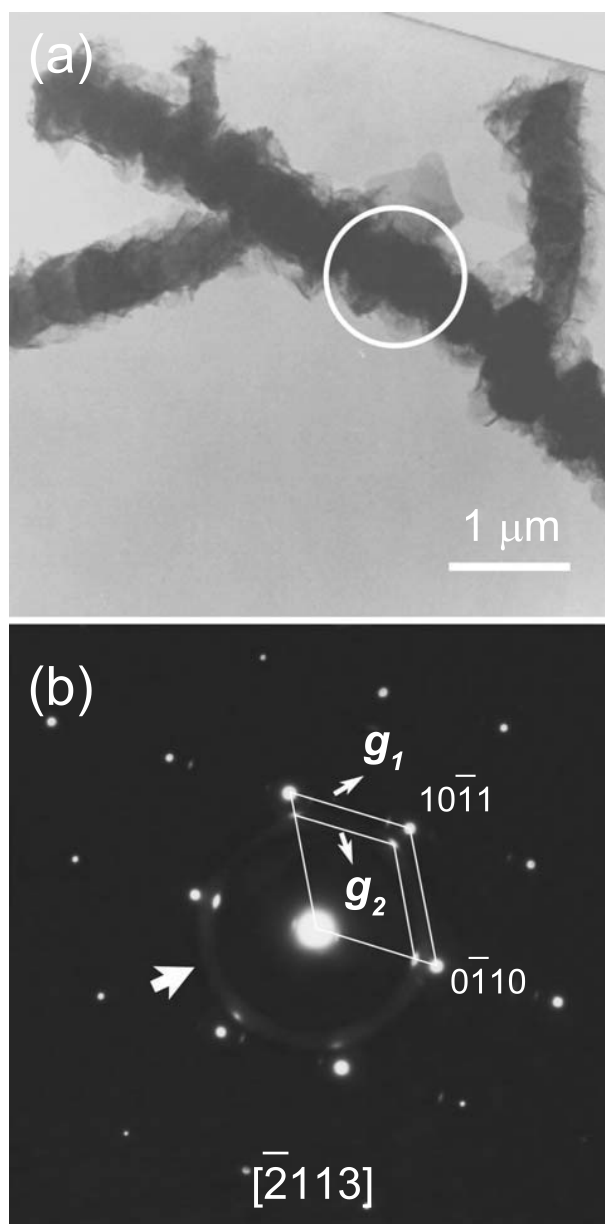
FIG. 3. (a) Diffraction contrast micrograph of the electrodeposit branch with a TEM. (b) The electron diffraction pattern obtained in the circle indicated in (a). Two sets of diffraction spots can be identified. The brighter diffraction spots indicated by g_1 correspond to zinc, whereas the spots indicated by g_2 correspond to zinc oxide. The incidence of the electron beam is from $[\bar{2}113]$.

tively, and the results are shown in Figs. 4(b)–4(d). In the kernel part the oxygen signal is very weak compared to that of zinc. On the part of platelets, however, the ratio of oxygen and zinc becomes much higher, as shown in Fig. 4(d). Therefore, it is quite possible that the scalelike platelets are ZnO. To verify this result, transmission electron microscopy is used to determine the structure and the orientation of the platelets. Figures 5(a) and 5(b) illustrate the TEM micrographs of an electrodeposit filament covered with platelets and the electron diffraction pattern of a platelet only. Figure 5(b) indicates that the scalelike platelet is ZnO with orientation $[\bar{2}110]$. We therefore conclude that the regularly angled
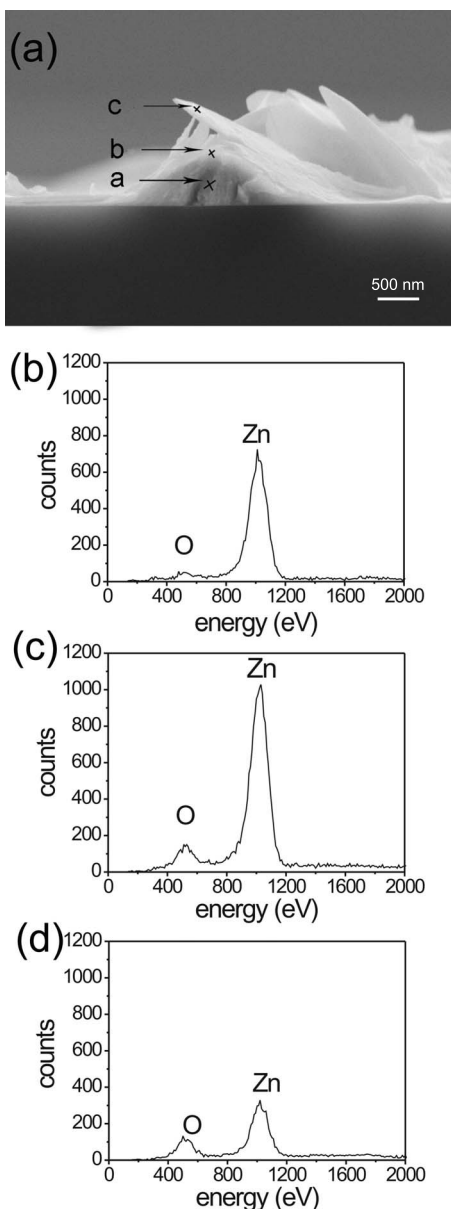
FIG. 4. (a) Scanning electron micrograph of the cross section of an electrodeposit branch grown on silicon wafer. It is clear that the electrodeposit branch has a compact kernel, which is covered with randomly oriented platelets. (b) EDS analysis made on the kernel part of the branch, site *a*, as indicated in (a). The signal of oxygen is very weak. (c) EDS analysis made on site *b*, as indicated in (a). (d) EDS analysis made on site *c*, in the region with random platelets, as indicated in (a). The strength of the signals of oxygen and zinc becomes comparable.

branches are single-crystalline zinc, covered with epitaxially grown platelets of ZnO.

III. DISCUSSIONS

To understand how the unique structure presented above is generated, we first need to resolve why the single-crystalline zinc trunks are bounded with ZnO platelets.

Electrocrystallization of zinc can be generally understood as follows. Zn^{2+} ions are driven to the cathode by the electric field; they are then reduced and diffuse on the deposit surface. Nucleation of the adsorbed atoms, followed by limited growth, gives rise to a crystallite agglomerate. According to the Nernst equation, the equilibrium electrode potential of $Zn|Zn^{2+}$ increases when the concentration of Zn^{2+} ($[Zn^{2+}]$) builds up. The electrodeposition of zinc takes place only when the potential of the cathode is lower than this equilibrium value. The equilibrium electrode potential for ZnO, however, is higher than that for Zn [35]. So, for a wide range of electrolyte concentrations, ZnO deposits with priority. Suppose $[Zn^{2+}]$ is initially high at the growing interface, and the equilibrium potential for zinc deposition is also high. By applying a sufficiently low electrode potential, both Zn and ZnO are deposited on the cathode, following the routes

$$Zn^{2+} + 2e^- \rightarrow Zn,$$

$$Zn^{2+} + \tfrac{1}{2}O_2 + 2e^- \rightarrow ZnO.$$
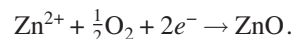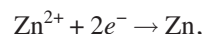
On the other hand, it should be noted that the deposition rate of ZnO is proportional to the product of both $[Zn^{2+}]$ and the concentration of dissolved oxygen in the electrolyte, whereas the oxygen concentration in the electrolyte solution is generally much lower than $[Zn^{2+}]$. Therefore, the mass deposition rate of ZnO is low compared to that of zinc. So in electrodeposition a zinc trunk with little ZnO is formed first. As the tips of the deposit filaments grow forward, $[Zn^{2+}]$ adjacent to the rear part of the filaments becomes lower. Once the concentration of Zn^{2+} becomes sufficiently low in the rear part of the filament, deposition of zinc is stopped, whereas the deposition of ZnO remains. In this way, ZnO platelets cover the zinc trunks.

There may exist a parallel mechanism for the generation of ZnO and launching oscillatory growth during the zinc electrodeposition. As electrodeposition of zinc continues, concentration of Zn^{2+} is gradually depleted in front of the growing interface, which slows down the zinc deposition, and possibly consumes H^+ in the solution (it has indeed been reported that hydrogen exists in electrodeposits of zinc [36]). For this reason, the *p*H around the electrodeposits is locally shifted to a higher value, which leads to the formation of ZnO. When this happens, the potential at the cathode/solution interface locally shifts to a more positive value, mainly due to the increased resistance of semiconducting ZnO over Zn (the depletion of Zn^{2+} concentration also contributes to this effect). The deposition of zinc oxide proceeds until the *p*H around the deposit tips returns to the nearby bulk value (a diffusion-driven process). Once the *p*H and concentration of Zn^{2+} in front of the electrodeposits resume previous values, ZnO growth stops, and Zn deposition restarts.

To check our explanations, we prepared $ZnSO_4$ aqueous solution and bubbled it with nitrogen gas for 24 h, with the aim of removing oxygen dissolved in the solution as much as possible. The electrodeposits generated in this specially treated solution are shown in Fig. 6. It can be seen that the randomly oriented platelets disappear, and layer-grown
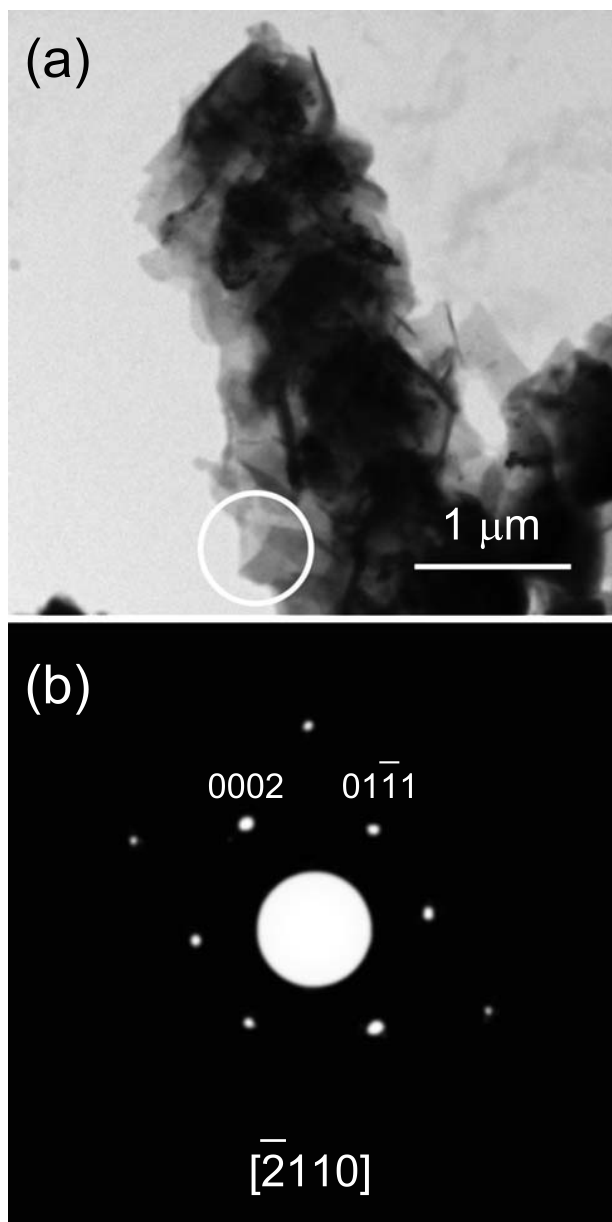
FIG. 5. (a) Diffraction contrast micrograph of the electrodeposit branch observed with TEM. The solid kernel is bounded with scale-like platelets. (b) The electron diffraction pattern obtained in the circled region, suggesting that the platelet is indeed ZnO.

FIG. 6. SEM micrograph of the electrodeposit branch when the electrolyte solution is nitrogen bubbled for a long time. No scalelike platelets are observed on the deposit branch.

roughly 60° (120°), as shown in Fig. 7(a). Bearing in mind that the ZnO platelets and the zinc trunk have single-crystalline electron diffraction patterns and take the same crystallographic orientation [see Fig. 3(b)], we suggest that
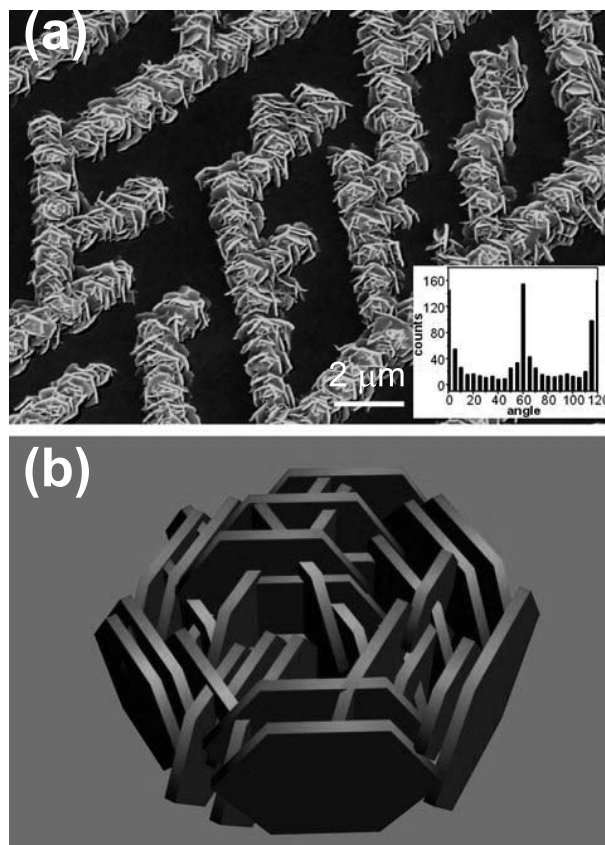
FIG. 7. (a) SEM micrograph of the electrodeposit branches covered with scalelike platelets. The insert illustrates the statistics of the angle between the platelets. Distinct peaks appear at 0°, 60°, and 120°. (b) The schematic diagram to illustrate "randomly" orientated ZnO platelets. These random-looking platelets essentially bear the identical crystallographic orientation.

zinc branches are generated. The periodic structure on the zinc branch (periodic clustering of ZnO platelets) probably results from the oscillation of the concentration field of $[Zn^{2+}]$ in the ultrathin aqueous solution film, similar to what happened in copper electrodeposition, as we reported before [25,26].

It is a challenge to understand the relation of the crystallographic orientation of the zinc trunk and the random-looking zinc oxide platelets. It is known that zinc has a hexagonal close-packed structure, with $a=b=2.66$ Å, $c=4.94$ Å. Zinc oxide also forms in a hexagonal closed-packed structure, with $a=b=3.249$ Å, $c=5.205$ Å. When we examine the surface morphology of the electrodeposits, we find that the angle between the neighboring platelets is

the ZnO platelets are epitaxially grown on the single-crystalline zinc trunk. According to the structural parameters and the symmetry of ZnO, we suggest that the platelet of ZnO is constructed by $\{0001\}$, $\{10\bar{1}1\}$, $\{10\bar{1}\ \bar{1}\}$, $\{1\bar{2}10\}$, with $\{1\bar{2}10\}$ being the top and 'bottom' faces, and $\{0001\}$, $\{10\bar{1}1\}$, and $\{10\bar{1}\ \bar{1}\}$ being the side faces. Suppose the zinc trunk of the electrodeposits is bounded by $\{10\bar{1}1\}$ and $\{0001\}$ faces, as suggested in Fig. 7(b). It follows that the ZnO crystallites may *epitaxially* nucleate on zinc with some degree of mismatch. Once this process occurs, the total free energy of the system stays low, and a cluster similar to that shown in Fig. 7(b) appears, which is similar to the experimental observation. In this way, the crystallographic orientation of the crystallites is identical [Fig. 3(b)], even though the platelets appear to be randomly orientated.

To summarize, we report here a long-range ordering effect in electro-crystallization of Zn and ZnO from an ultrathin aqueous electrolyte layer of $ZnSO_4$. The deposit branches are regularly angled, covered with random-looking, scalelike platelets of ZnO. Our experiments show that ZnO platelets are epitaxially grown on the zinc trunk and possess the same crystallographic orientation. To epitaxially nucleate on the zinc trunk, ZnO crystallites selectively contact the $[\bar{2}113]$-orientated zinc substrate with $\{0001\}$, $\{10\bar{1}1\}$, and $\{10\bar{1}\ \bar{1}\}$ faces. In this way, the crystalline platelets possess the same crystallographic orientation as the zinc trunk. We suggest that such a crystallization behavior should be enlightening in understanding the formation process of many patterns in interfacial growth.

[1] M. Matsushita, M. Sano, Y. Hayakawa, H. Honjo, and Y. Sawada, Phys. Rev. Lett. **53**, 286 (1984).

[2] F. Sagues, M. Q. Lopez-Salvans, and J. Claret, Phys. Rep. **337**, 97 (2000).

[3] V. Fleury and D. Barkey, Physica A **233**, 730 (1996).

[4] S. N. Atchison, R. P. Burford, and D. B. Hibbert, J. Electroanal. Chem. **371**, 137 (1994).

[5] D. P. Barkey, D. Watt, Z. Liu, and S. Raber, J. Electrochem. Soc. **141**, 1206 (1994).

[6] J. R. Melrose, D. B. Hibbert, and R. C. Ball, Phys. Rev. Lett. **65**, 3009 (1990).

[7] O. Zik and E. Moses, Phys. Rev. E **53**, 1760 (1996).

[8] V. Fleury, J. Kaufman, and D. B. Hibbert, Nature (London) **367**, 435 (1994).

[9] M. Wang, W. J. P. van Enckevort, N.-B. Ming, and P. Bennema, Nature (London) **367**, 438 (1994).

[10] J. Huth, H. Swinney, W. McCormick, A. Kuhn, and F. Argoul, Phys. Rev. E **51**, 3444 (1995).

[11] W. G. Huang and D. B. Hibbert, Physica A **233**, 888 (1996).

[12] O. Younes, L. Zeiri, S. Efrima, and M. Deutsch, Langmuir **13**, 1767 (1997).

[13] J. R. Melrose, D. B. Hibbert, and R. C. Ball, Phys. Rev. Lett. **65**, 3009 (1990).

[14] M. Rosso, E. Chassaing, and J.-N. Chazalviel, Phys. Rev. E **59**, 3135 (1999).

[15] J. Elezgaray, C. Leger, and F. Argoul, Phys. Rev. Lett. **84**, 3129 (2000).

[16] S. Bodea, L. Vignon, R. Ballou, and P. Molho, Phys. Rev. Lett. **83**, 2612 (1999).

[17] C. Leger, F. Argoul, and M. Z. Bazant, J. Phys. Chem. B **103**, 5841 (1999).

[18] J. L. Hudson, Chem. Eng. Sci. **49**, 1493 (1994).

[19] F. Argoul and A. Kuhn, J. Electroanal. Chem. **359**, 81 (1993).

[20] H. D. Dewald, J. Electrochem. Soc. **140**, 1969 (1993).

[21] J. A. Switzer, C. J. Hung, L. Y. Huang *et al.*, J. Mater. Res. **13**, 909 (1998).

[22] S. Nakanishi, K. Fukami, T. Tada, and Y. Nakato, J. Am. Chem. Soc. **126**, 9556 (2004).

[23] K. Fukami, S. Nakanishi, T. Tada *et al.*, J. Electrochem. Soc. **152**, C493 (2005).

[24] S. Leopold, M. Herranen, and J. O. Carlsson, J. Electrochem. Soc. **148**, C513 (2001).

[25] M. Wang, S. Zhong, X. B. Yin, J. M. Zhu, R. W. Peng, Y. Wang, K. Q. Zhang, and N. B. Ming, Phys. Rev. Lett. **86**, 3827 (2001).

[26] S. Zhong, Y. Wang, M. Wang, M. Z. Zhang, X. B. Yin, R. W. Peng, and N. B. Ming, Phys. Rev. E **67**, 061601 (2003).

[27] M. Wang and N.-B. Ming, Phys. Rev. Lett. **71**, 113 (1993).

[28] M. Wang and N.-B. Ming, Phys. Rev. A **45**, 2493 (1992).

[29] D. Grier, E. Ben-Jacob, R. Clarke, and L. M. Sander, Phys. Rev. Lett. **56**, 1264 (1986).

[30] S. Wang, K.-Q. Zhang, Q.-Y. Xu, M. Wang, R.-W. Peng, Z. Zhang, and N.-B. Ming, J. Phys. Soc. Jpn. **72**, 1574 (2003).

[31] Ivan V. Markov, *Crystal Growth for Beginners: Fundamentals of Nucleation, Crystal Growth and Epitaxy* (World Scientific, Singapore, 1998).

[32] X. Y. Liu and C. S. Strom, J. Chem. Phys. **113**, 4408 (2000).

[33] N.-B. Ming, *Fundamentals of Crystal Growth Physics* (Shanghai Science and Technology Press, Shanghai, 1982).

[34] Y. Wang, Y. Cao, M. Wang, S. Zhong, M.-Z. Zhang, Y. Feng, R.-W. Peng, X.-P. Hao, and N.-B. Ming, Phys. Rev. E **69**, 021607 (2004).

[35] The standard electrode potential of $Zn|Zn^{2+}$ is -0.76 V versus NHE while the standard electrode potential of $Zn|ZnO$ is 0.88 V versus NHE.

[36] D. G. Grier, K. Allen, R. S. Goldman, L. M. Sander, and R. Clarke, Phys. Rev. Lett. **64**, 2152 (1990).